Collision Energy Dependence of the $O(^1D) + HCl \rightarrow OH + Cl(^2P)$ Reaction Studied by Crossed Beam Scattering and Quasiclassical Trajectory Calculations on Ab Initio Potential Energy Surfaces

Hiroshi Kohguchi and Toshinori Suzuki*

Chemical Dynamics Laboratory, RIKEN, Hirosawa 2-1, Wako 351-0198, Japan

Shinkoh Nanbu

Research Institute for Information Technology, Kyusyu University, Hakozaki, Higashiku, Fukuoka 812-8581, Japan

Toshimasa Ishida

Fukui Institute for Fundamental Chemistry, Kyoto University, Takano-nishihirakicho, Sakyoku, Kyoto 606-8103, Japan

Gennady V. Mil'nikov,† Ponmile Oloyede,‡ and Hiroki Nakamura

Institute for Molecular Science, Myodaiji, Okazaki 444-8585, Japan

Received: August 15, 2007; In Final Form: October 31, 2007

The dynamics of the $O(^1D) + HCl \rightarrow OH + Cl(^2P)$ reaction are investigated by a crossed molecular beam ion-imaging method and quasiclassical trajectory calculations on the three ab initio potential energy surfaces, the ground $1^1A'$ and two excited ($1^1A''$ and $2^1A'$) states. The scattering experiment was carried out at collision energies of 4.2, 4.5, and 6.4 kcal/mol. The observed doubly differential cross sections (DCSs) for the $Cl(^2P)$ product exhibit almost no collision energy dependence over this inspected energy range. The nearly forward−backward symmetric DCS indicates that the reaction proceeds predominantly on the ground-state potential energy surface at these energies. Variation of the forward−backward asymmetry with collision energy is interpreted using an osculating complex model. Although the potential energy surfaces obtained by CASSCF-MRCI ab initio calculations exhibit relatively low potential barriers of 1.6 and 6.5 kcal/mol for $1^1A''$ and $2^1A'$, respectively, the dynamics calculations indicate that contributions of these excited states are small at the collision energies lower than 15.0 kcal/mol. Theoretical DCSs calculated for the ground-state reaction pathway agree well with the observed ones. These experimental and theoretical results suggest that the titled reaction at collision energies less than 6.5 kcal/mol is predominantly via the ground electronic state.

Introduction

The interaction of atomic oxygen in the first excited singlet state [$O(^1D)$] with a closed-shell hydride (MH) gives rise to five electronic states at close distance. Among them, the minimum-energy path leads to a deep potential well at the M−O−H geometry, which corresponds to stable intermediates such as $H_2O(X\ ^1A_1)$ and $CH_3OH(X\ ^1A')$ in the $O(^1D) + H_2$ and $O(^1D) + CH_4$ reactions, respectively. Meanwhile, the excited-state potential energy surfaces (PESs) of these intermediates have energy barriers for bimolecular reactions.[1−5] The large reactivity of $O(^1D)$ results from the attractive interactions on the ground-state PES, while the repulsive excited-state PESs may contribute at higher collision energy (E_{col}). These are qualitatively common features of the PESs for the $O(^1D) + MH$ reactions. Opening of the excited-state reaction pathway at an elevated collision energy has been identified by the crossed molecular beam study and the theoretical calculations for the $O(^1D) + H_2$ (and its isotope variants) reaction.[6−8] The excitation function observed by Hsu et al. declined with E_{col} up to ∼1.8 kcal/mol and then gradually increased above this energy.[8] The declining reactive cross section, $\sigma_{reac}(E_{col})$, is a typical attribute to attractive PESs with no energy barrier, while the slow rise is attributed to a PES with an energy barrier. The energy threshold of the latter channel is in good agreement with the barrier height of 2.3 kcal/mol at the H−H−O collinear configuration obtained by the ab initio calculation by Schatz et al.[9] Their calculations predicted a comparable barrier height and reactivity for the $1^1A''$ and $2^1A'$ states. The energy dependence of the angle-specific translational energy release, or doubly differential cross section (DCS),[6,7] unambiguously showed the contribution of the excited state PES(s); the forward−backward symmetric DCS below the energy threshold is ascribed to the pure insertion mechanism on the $1^1A'$ PES,[10] while the increasing backward components at higher E_{col} is interpreted as a manifestation of abstraction mechanism due to the excited $1^1A''$ and/or $2^1A'$ state PESs.[6,7]

* To whom correspondence should be addressed. E-mail: toshisuzuki@riken.jp.

† Current address: Faculty of Engineering, Osaka University, Suita 565-0871, Osaka, Japan

‡ Current address: Department of Chemistry and Environmental Science, New Jersey Institute of Technology, University Heights, Newark, New Jersey 07102.

10.1021/jp076581x CCC: $40.75
Published on Web 01/12/2008

The $O(^1D) + HCl \rightarrow OH + Cl$ system also forms a deep insertion well on the ground-state PES ($1^1A'$) corresponding to the hypochlorous acid (HOCl) molecule. Although a part of the excited-state PES(s) responsible for ultraviolet (UV) photodissociation of HOCl has been theoretically studied,[11−14] global PESs of the $1^1A''$ and $2^1A'$ states relevant to the titled reaction were investigated only recently.[15] Previous experimental studies have pointed only to the ground-state ($1^1A'$) dynamics. Park and Wiesenfeld measured the vibrational and rotational state distributions of OH products by laser-induced fluorescence (LIF) spectroscopy, and they suggested the reaction mechanism solely on the ground-state PES on the basis of the observed unimodal triangle plot of energy disposal (rotational, vibrational, and translational energy release).[16] Matsumi and co-workers measured the branching ratio between the OH + Cl and ClO + H pathways together with their isotope effects (H and D) and the kinetic energy releases.[17] They also argued that the primary reaction pathways of both product channels are the $1^1A'$ ground-state PES; yet, the products are controlled by orientation of HCl with respect to the incoming O atom; a sideway attack of $O(^1D)$ to HCl leads to OH + Cl by an insertion/decomposition mechanism, while the initial approach of $O(^1D)$ to the Cl end results in ClO production due to abstraction, both on the ground-state PES. For the ClO production, an abstraction mechanism through the excited $1^1A''$ PES was proposed as another possibility by Kruus et al.[18] from their time-resolved Fourier transform chemiluminescence spectroscopy. The doubly DCS of the OH + Cl pathways was measured for each of the $Cl(^2P_{J=3/2})$ and $Cl^*(^2P_{J=1/2})$ products by our previous crossed beam study at $E_{col} = 6$ kcal/mol.[19] The angular distributions exhibit pronounced preference in the forward direction. Although any evidence of the contribution of the excited-state PESs was not seen in the experimental observables, further investigation at different collision energies has been performed to elucidate the influence of the excited states.

The detailed structure of the ground-state ($1^1A'$) PES has been examined in theoretical studies. In addition to the potential well at the O-insertion geometry (HOCl), another shallower potential well associated with the HClO configuration has been confirmed by the ab initio studies for the $1^1A'$ PES.[11,12,15,20−22] These ab initio data for the $1^1A'$ PES have been applied to the dynamics calculations.[23−35] Although the global PESs of the excited states ($1^1A''$ and $2^1A'$) have been calculated by Nanbu et al. with the same accuracy as that of the ground state,[15] the dynamics calculations on these PESs were limited only to $\boldsymbol{J}$ (total angular momentum) = 0.[24,25] The ab initio calculations predicted comparable or even lower reaction barriers of the excited-state PESs than the E_{col} applied in our previous study. Here, we present the experimental and theoretical studies to explore the role of the excited-state dynamics in the $O(^1D) + HCl \rightarrow OH + Cl(^2P)$ reaction. Scattering distributions observed by crossed beam ion imaging at three collision energies are compared with quasiclassical trajectory (QCT) calculations executed on the $1^1A''$ and $2^1A'$ excited-state PESs as well as on the $1^1A'$ ground state.

Experimental Section

The details of the experimental setup are described elsewhere.[19] In the present experiment, we varied the speed of the HCl molecular beam by using He, Ne, and Ar as carrier gases. The HCl was diluted in each carrier gas by 5% in concentration. The time profile of the pulsed HCl molecular beam was measured by a fast ion gauge (FIG-1, Beam Dynamics, Inc.) 140 and 280 mm downstream from the collision center. We determined the HCl beam speed from the difference in arrival times between these two positions to be 1398 ± 118 m/s in He, 729 ± 58 m/s in Ne, and 531 ± 40 m/s in Ar. These beam speeds yield E_{col} of 6.4 (1.4), 4.5 (0.8), and 4.2 (0.7) kcal/mol for the He, Ne, and Ar carrier gases, respectively. The collision energy spread (ΔE_{col}: full width at half-maximum) in the parentheses is evaluated from the velocity width of each HCl beam and the $O(^1D)$ beam. The Newton diagrams at each E_{col}, which are constructed from the beam characterization, are employed for image data analysis.

The $O(^1D)$ beam was generated by F_2 laser photolysis at 157 nm (LPF 220, Lambda Physik) of the O_2 precursor (1% O_2 in He). The scattering $Cl(^2P_{3/2})$ signal was detected with the UV probe laser pulse of 200 μJ/pulse. The lower probe laser intensity than that in our previous study (400 μJ/pulse) suppressed the one-color dissociation/ionization noise from the HCl target beam; the spot-like HCl^+ noise image is less than 5% of the Cl^+ signal from the titled reaction, which is sufficiently small to obviate subtraction of this particular noise image from the signal image. As shown later, we still needed subtracting of another type of noise arising from the O atom beam source. The count rate of the Cl^+ signal from the reactive scattering was ∼20 counts per laser shot at most. The probe laser wavelength was scanned over 2.7 cm^{-1} around the two-photon resonant line of $Cl(^2P_{3/2}) \rightarrow Cl(^2D_{3/2})$ at 235.326 nm. This scanning range covers the Doppler components of ±9500 m/s, which is sufficiently wide to detect the entire range of scattering velocities. The images of Cl^+ at each E_{col} are accumulated for ∼1 h. These images at the three E_{col} are measured under the same detection conditions. The signal intensities with the Ne-seeded ($E_{col} = 4.5$ kcal/mol) and the Ar-seeded ($E_{col} = 4.2$ kcal/mol) HCl beams are ∼80 and ∼40% of that with the He-seeded HCl sample ($E_{col} = 6.4$ kcal/mol), respectively. These ratios do not correctly reflect the $\sigma_{reac}(E_{col})$ but the difference of the effective HCl beam density with the carrier gases (He, Ne, and Ar). Resultantly, the signal-to-noise ratio of the present data decreases in the descending order of the collision energy.

The observed image is 2D projection data of a 3D density distribution of the $Cl(^2P_{3/2})$ products at the instance of laser irradiation. The first step of image data analysis is density-flux transformation using an apparatus function given by the temporal and geometrical configurations of the pulsed atomic/molecular beams and the laser beam.[36] The apparatus function was numerically simulated with the experimental parameters describing the spatial and temporal profiles of the atomic/molecular beams and the laser beam. The degree of correction in the density-flux transformation was rather small, as the velocity of the Cl product (v_{Cl}) in this reaction was relatively small (maximum $v_{Cl} < 1800$ m/s). The doubly (velocity-angle) DCSs are obtained for the three E_{col} values by an inverse Abel transform of the density-flux corrected images.

Theoretical Calculation

The global PESs of the $1^1A'$, $1^1A''$, and $2^1A'$ states were obtained in our previous study by ab initio calculation implemented with the CASSCF-MRCI method by the MOLPRO suite of programs.[37] The detail of the quantum chemistry calculation is described in the original paper.[15] The MRCI calculation was executed on 4631 molecular geometries; the ranges of the bond lengths are $R(O-H) = 0.6-5.0$ Å, $R(Cl-O) = 1.2-6.0$ Å, and $R(H-Cl) = 0.8-5.0$ Å. The interpolant moving least-squares method combined with Shepard interpolation developed by Ishida and Schatz[38] was applied to generate the fitted global PESs, which are employed for the present QCT dynamical

calculations. The QCT calculations are carried out independently on the $1^1A'$, $1^1A''$, and $2^1A'$ adiabatic PESs at E_{col}'s of 3.0, 4.0, 6.0, 12.2, and 15.0 kcal/mol. The range of $E_{col} = 3.0-6.0$ kcal/mol is chosen for comparison with the experimental data, while the trajectories at higher E_{col} are also examined for further surveillance of the E_{col} dependence of the excited-state dynamics. The couplings between these PESs are not taken into account. Each trajectory is run with a specific E_{col} for the $(v, j) = (0, 0)$ rovibrational state of HCl. All other variables specifying the initial conditions are chosen randomly by Monte Carlo sampling. The equation of motion was integrated by the fourth-order Runge−Kutta method on each adiabatic PES. Propagation of the trajectory was terminated when one of the three internuclear distances exceeded 8 Bohr (4.23 Å). The number of the trajectories was ~20 000 for each PES. The destinations of the trajectories are grouped into the OH + Cl, ClO + H, and O + HCl (inelastic) pathways. Among them, the trajectories ending with the OH + Cl pathway are compared with the experimental results.

Results and Discussion

A. Scattering Experiment. The ion images of the $Cl(^2P_{3/2})$ product observed at the collision energies of 6.4, 4.5, and 4.2 kcal/mol are shown in Figure 1a, b, and c, respectively. The images are placed so that the collision axis (thin black line) is aligned upright. The Newton diagram is superimposed on each image, where the velocity vectors of the HCl and the $O(^1D)$ beams are depicted by thick arrows. The center-of-mass velocity is shown by a thin arrow, whose end points at the center-of-mass. The spot-like noise, which is due to byproducts contaminated in F_2 laser photolysis, is seen at the end of the $O(^1D)$ beam velocity vector. This noise image is eliminated prior to image data analysis. The production of the $Cl^*(^2P_{1/2})$ is a minor spin−orbit pathway in the present collision energy region.[17,39] In addition, it seems that the spin−orbit branching can occur in the asymptotic product (OH + Cl) region;[19] therefore, both of the excited- and ground-state reaction channels can be monitored by $Cl(^2P_{3/2})$. This gives us some justification for using the data of $Cl(^2P_{3/2})$ to discuss the overall reaction dynamics on the ground and excited electronic states in the rest of this paper.

The center-of-mass translational energy releases, $P(E_t)$, obtained from these images are shown in Figure 2a for an E_{col} of 6.4 kcal/mol, in b for 4.5 kcal/mol, and in c for 4.2 kcal/mol. The available energies (E_{avl}) are almost the same, (a) 17 800, (b) 17 100, and (c) 17 000 cm^{-1}, because of a large exothermicity of the reaction. Correspondingly, the obtained average translational energy release $[\langle E_t \rangle = \sum E_t P(E_t)/P(E_t)]$ is similar for the three cases, that is, (a) 3830 (170), (b) 3820 (270), and (c) 3590 (210) cm^{-1} for $E_{col} = 6.4$, 4.5, and 4.2 kcal/mol, respectively. The values in the parentheses are the differences between the results with/without sensitivity correction for the observed images, which were found to be unimportant in the following discussion. The observed $P(E_t)$ values at the three E_{col}'s yield a small energy partitioning to the translational energy ($\langle f_T \rangle$) of 22 ± 2%, exhibiting formation of highly internally excited OH. The strong internal excitation of OH has been well-known both in the experimental[16,18,19,40,41] and theoretical[23−29,33−35,42] studies as a distinctive attribute of the $O(^1D)$ + HCl reaction. Our $P(E_t)$ agrees very well with the state distribution of the counterpart product OH reported by Park and Wiesenfeld.[16] For comparison, we calculated $P(E_t)$ from the triangular plot reported by Park and Wiesenfeld, as presented in a dashed curve in Figure 2a. Note that their experiment was carried out with a rather broad collision energy spread (average $E_{col} = 7$ kcal/mol), while the present experiment was carried out at a well-defined collision energy. Despite this difference in conditions, the $P(E_t)$'s distribute mostly in the low E_t (<10 000 cm^{-1}) region in both cases and are consistent with each other.

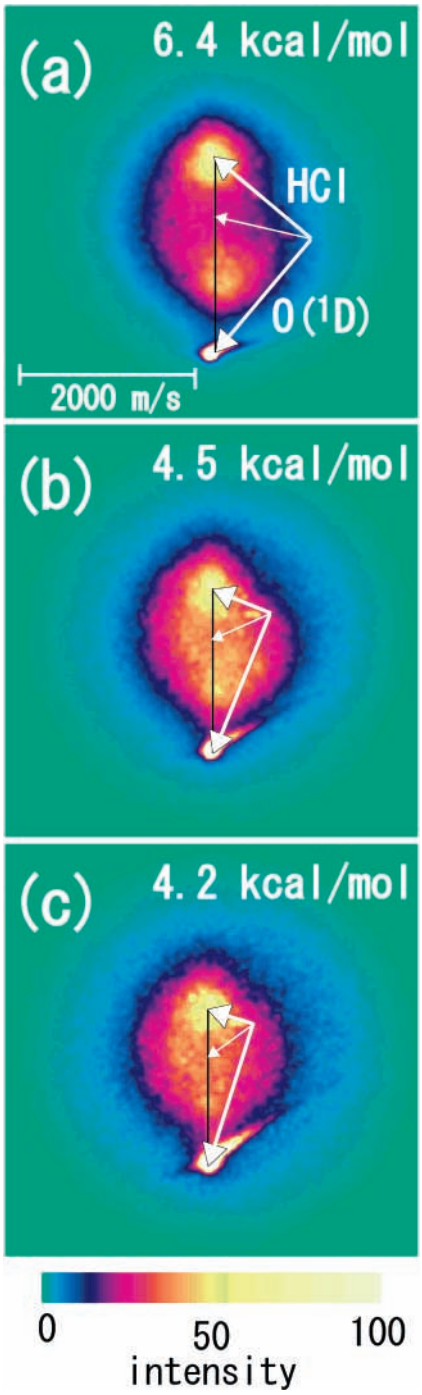

Figure 1. Observed scattering images of $Cl(^2P_{3/2})$ products in the $O(^1D)$ + HCl → OH + Cl reaction. The collision energies are (a) 6.4, (b) 4.5, and (c) 4.2 kcal/mol. The geometry of the HCl and $O(^1D)$ beams is shown by the Newton diagram superimposed in each image. The HCl and $O(^1D)$ beam velocity vectors, which are crossed at right angles, are designated by the thick arrows. The center-of-mass velocity shown by a thin arrow points to the scattering center on the collision axis, which is represented by a vertical black line. The spot-like noise at the end of the $O(^1D)$ beam velocity is due to byproducts in laser photolysis. The direction of the probe laser beam bisects the included right angle between the HCl and the $O(^1D)$ beams in all images.

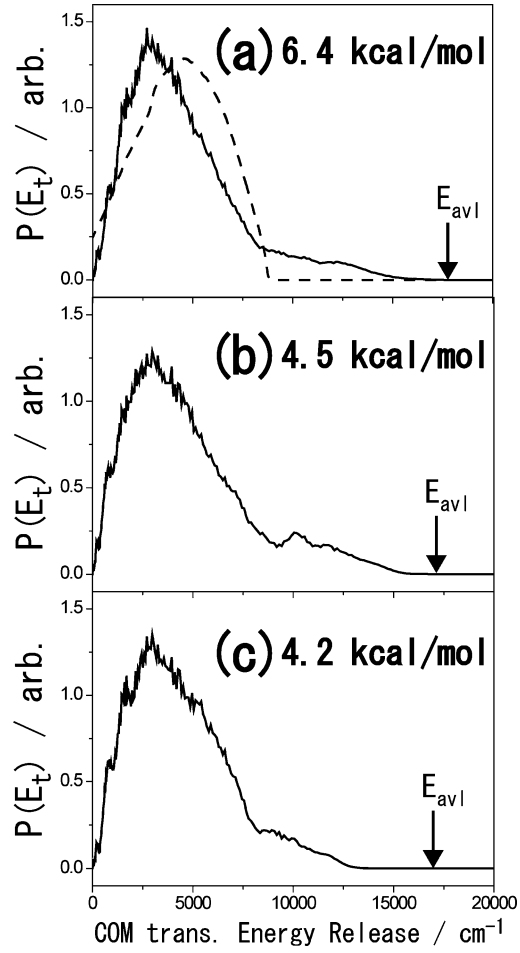

Figure 2. The center-of-mass translational energy release of the $O(^1D) + HCl \rightarrow OH + Cl$ reaction at the collision energies (E_{col}) of (a) 6.4, (b) 4.5, and (c) 4.2 kcal/mol. The dashed curve in (a) is obtained from the rovibrational state distribution of OH measured by Park and Wiesenfeld,[16] for which the translational energy was determined for the average collision energy of 7.4 kcal/mol. All of the scattering angular components are integrated. All of the graphs are normalized to have a certain common area. The available energies ($E_{avl} = \Delta H + E_{col}$) are denoted by an arrow in each plot.

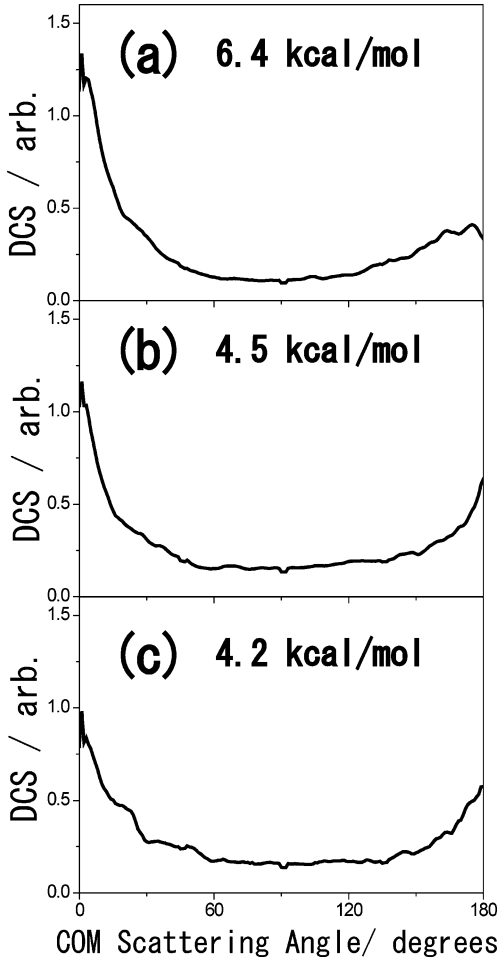

Figure 3. The differential cross section of the $O(^1D) + HCl \rightarrow OH + Cl$ reaction at the collision energies of (a) 6.4, (b) 4.5, and (c) 4.2 kcal/mol. All of the scattering velocity components are integrated. All of the graphs are normalized to have a certain common area for comparison.

The DCSs extracted from the slice (Abel inverted) image data at the three E_{col}'s are presented in Figures 3a−c. These are the angular distributions integrated over the whole scattering velocity (or E_t) component at $E_{col} = 6.4$ kcal/mol (Figure 3a), 4.5 kcal/mol (Figure 3b), and 4.2 kcal/mol (Figure 3c). As is expected from the observed images (Figure 1), the DCSs at the three E_{col}'s are peaking in the forward and backward directions, while the sideways components with the center-of-mass scattering angle (θ_{cm}) from 30 to 150° amount to less than 50% of the total intensity. The DCS at $E_{col} = 6.4$ kcal/mol (Figure 3a) shows pronounced preference for forward scattering; the intensity of the forward components ($0 < \theta_{cm} < 30°$) is more than twice the backward ($150 < \theta_{cm} < 180°$) ones. The preference slightly decreases in the lower E_{col} (4.5 kcal/mol in Figure 3b and 4.2 kcal/mol in Figure 3c). The DCSs at $E_{col} =$ 4.2 and 4.5 kcal/mol, which are overlapped each other within the ΔE_{col}, are almost identical, except for the lower signal statistics of the data with the Ar buffer beam ($E_{col} = 4.2$ kcal/mol). The observed preference of the forward scattering with the increasing E_{col} is explained by the osculating complex model for chemical reactions.[43,44] The model provides an estimate of the reaction time (τ_{reac}), which is a fraction of, or comparable to, the rotational period of the complex (τ_{rot}) by the relation of $T(\theta_{cm} = 180°)/T(\theta_{cm} = 0°) = \exp(-\tau_{rot}/2\tau_{reac})$, where $T(\theta_{cm})$ is the experimental DCS. The rotational period of $\tau_{rot} = 2\pi I/l_{eff}$ is evaluated by assuming the moment of inertia (I) at the equilibrium geometry of the HOCl or HClO potential well and the effective angular momentum of $l_{eff} = \mu v_{rel} b_{peak}$, where μ is the reduced mass, v_{rel} is the relative velocity, and b_{peak} is the impact parameter (b) at which the opacity function [$P(b)$] without a factor of $2\pi b db$ is maximized. The moments of inertia of I(HOCl) = 35.0 amu Å^2 and I(HClO) = 29.4 amu Å^2 are obtained from the ab initio results by Nanbu et al.[15] The representative value of $b_{peak} = 2.5$ Å is used on the basis of the QCT results, which are discussed later. An almost identical value of b_{peak} is presented in the QCT study at $E_{col} = 12.2$ kcal/mol by Martínez et al.[23] The geometry at the HOCl well yields the evaluation of $\tau_{rot} = 360$, 430, and 440 fs for $E_{col} = 6.4$, 4.5, and 4.2 kcal/mol, respectively. Consequently, the osculating complex model provides $\tau_{reac} = 340$, 940, and 1070 fs for $E_{col} = 6.4$, 4.5, and 4.2 kcal/mol, respectively. The assumption of the collision complex at the HClO well geometry yields shorter τ_{reac} by ∼15% than those at the HOCl well for each E_{col} condition. The above estimation employs the moment of inertia of a stable molecule, while a short-lived collision complex undergoes a large-amplitude motion during chemical reaction. Therefore, this analysis should be regarded qualitatively. Despite such a limitation, the osculating complex model, which implicitly assumes the ground-state reaction, well explains the trend of E_{col} dependence of the observed DCS. Since the enhancement

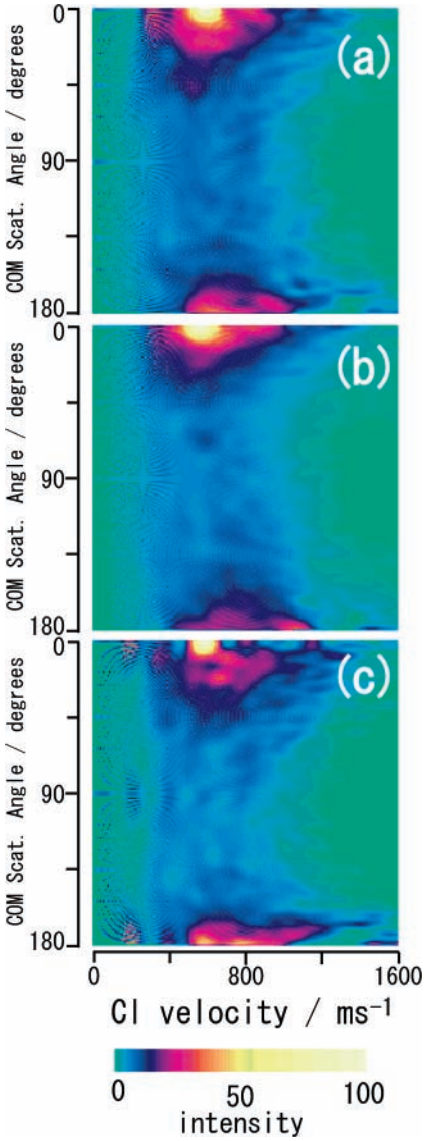

Figure 4. The doubly differential cross sections of the O(^{1}D) + HCl → OH + Cl reaction at the collision energies of (a) 6.4, (b) 4.5, and (c) 4.2 kcal/mol. The abscissa and ordinate represent the center-of-mass scattering angle and the product Cl velocity, respectively. The upward direction points to the forward component. A fixed pattern noise seen in the low-speed region (<400 m/s) is due to numerical artifact in the conversion of the small radius to the polar coordinate.

of the forward scattering at the higher E_{col} is considered to be a rather contrary indication to the contribution of the excited state PESs, the observed E_{col} dependence of the DCS confirms the dynamics predominantly on the ground-state PES. In addition, the preference of the forward components in all three E_{col}'s is in good agreement with the QCT results on the ground-state PES, as is described in the following section.

The doubly (θ_{cm} and v_{Cl}) DCSs in the polar coordinate representation are shown in Figure 4; E_{col} = 6.4 kcal/mol in Figure 4a, E_{col} = 4.5 kcal/mol in Figure 4b, and E_{col} = 4.2 kcal/mol in Figure 4c. An inaccurate intensity in the neighbors of θ_{cm} = 0 and 180° is unavoidable in the numerical Abel inversion. A fixed pattern noise, which is apparently seen in the slow speed region (v_{Cl} < 400 m/s) arises from the Cartesian-to-polar transformation of pixelized image data. These artifacts due to the numerical operations are neglected in the following discussion. The doubly DCSs in Figure 4a−c show the v_{Cl}−θ_{cm} correlation (nonseparability[45] of v_{Cl} and θ_{cm}), as is expected from the polarized (elongated) feature of the observed images

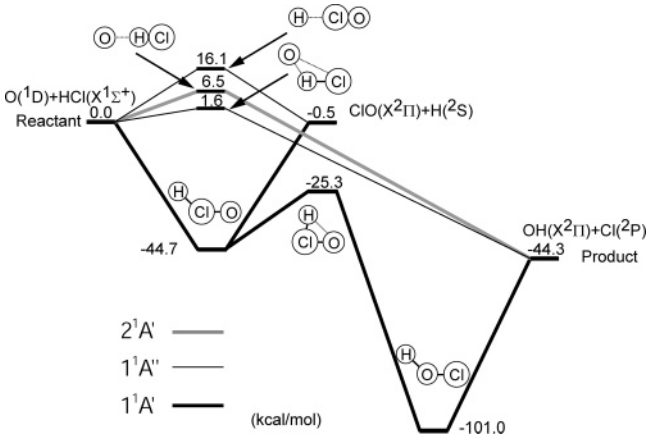

Figure 5. The schematic potential energy diagram of the O(^{1}D) + HCl reaction. The electronic energy for the saddle points and the equilibrium structures are shown in the units of kcal/mol. The electronic states correlating the saddle points and the equilibrium structures are designated by thick black lines for 1^1A′, thin black lines for 1^1A″, and thick gray lines for 2^1A′.

along the forward/backward directions. While the E_{col}-dependent forward−backward ratio is discussed in the former paragraph, no significant E_{col} dependence is found for the sideways components in the v_{Cl}−θ_{cm} plot. The polarized scattering distribution is presented in the previous experimental[19] and theoretical[23] studies of the O(^{1}D) + HCl reaction; the observed correlation between the forward θ_{cm} and the slow v_{Cl} is ascribed to a peripheral dynamics in which a light atom is transferred between two heavier atoms separated at a large distance, leading to strong excitation of OH and a forward scattering. The QCT calculations by Martínez et al.[23] on the 1^1A′ PES at E_{col} = 12.2 kcal/mol indicated the delayed emission of products in the backward direction with respect to the forward direction. In the osculating complex regime of an insertion reaction, the reaction time is a fraction of a rotational period. Our result indicates that back-scattered products have higher recoil velocity, indicating weaker internal excitation in OH.[19] The results accord well with the theoretical prediction by Martínez et al.,[23] if de-excitation of the OH stretching vibration occurs due to mode coupling within the lifetime of a collision complex that is still shorter than its rotational period (0.3 ps). Thus, all of the experimental results suggest that the ground-state reaction dominates the titled reaction at the three E_{col}'s, although these exceed the potential barrier heights predicted by the CASSCF-MRCI calculation, as is described in the next section.

B. Quasiclassical Trajectory Calculations on the Ab Initio PESs. We will briefly review the ab initio PESs on which QCT calculations were performed. The detailed discussion on the topography of the 1^1A″ and 2^1A′ excited-state PESs was made by Nanbu et al.[15] The schematic energy diagram is shown in Figure 5. Both of these PESs are globally repulsive, with no bound-state region except for a shallow van der Waals well on the 2^1A′ PES. The saddle point structures on the 1^1A″ and 2^1A′ PESs obtained by the ab initio calculations are shown in Figure 6. The 1^1A″ PES has a saddle point at a bent geometry; the two-dimensional contour plot of the electronic energy with a fixed H−Cl bond length of 1.31 Å is shown in Figure 6a. The saddle point is located at the OH bond length of R(O−H) = 1.70 Å and the O−H−Cl angle of 129°. The barrier height from the reactant arrangement is 1.6 kcal/mol. The 2^1A′ PES also has a saddle point but at the O−H−Cl linear configuration shown in Figure 6b. The barrier, whose height is 6.5 kcal/mol, is located at R(O−H) = 1.35 Å and R(H−Cl) = 1.34 Å. Another saddle point on the 1^1A″ PES is found at the H−Cl−O linear

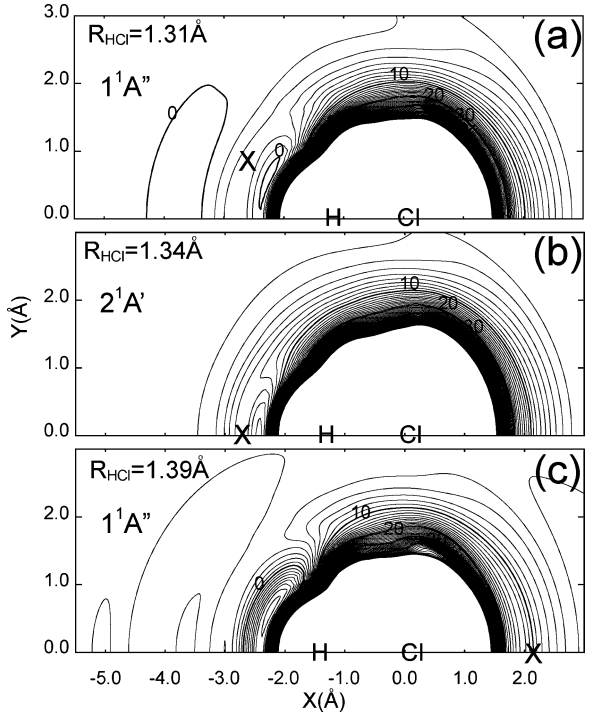

Figure 6. The contour plots of the electronic energy of the excited-state PESs at the fixed H−Cl bond length obtained by the ab initio calculation[15]: (a) the $1^1A''$ state with the fixed H−Cl bond length at 1.31 Å; (b) the $2^1A'$ state with the fixed H−Cl bond length at 1.34 Å; and (c) the $1^1A''$ state with the fixed H−Cl bond length at 1.39 Å. The saddle points are designated by × in each two-dimensional plot. The step of the energy contour is 1 kcal/mol. The saddle points in (a) and (b) represent the potential barriers from the O(^{1}D) + HCl reactant to the OH + Cl pathway. The saddle point in plot (c) shows the barrier from the reactant to the ClO + H pathway.

geometry. This is a saddle point from the reactant to the ClO + H pathway with the barrier height of 16.1 kcal/mol. The electronic energy around the saddle point is shown in Figure 6c.

The results of the QCT calculations executed on the $1^1A'$, $1^1A''$, and $2^1A'$ PESs are shown in Figures 7 and 8. The theoretical DCSs at various E_{col} are shown in Figure 7; the results on the $1^1A'$ are shown in Figure 7a, $1^1A''$ in 7b, and $2^1A'$ PESs in 7c. Unsmooth curves of the DCS of the excited states (Figure 7b and c) are due to the smaller number of resultant trajectories in the OH + Cl pathway than that of the ground state (Figure 7a). The overall feature of the QCT result on the $1^1A'$ PES (Figure 7a) is in good agreement with the observed DCS. The theoretical DCS on the ground-state PES exhibits the polarized distribution peaked at $\theta_{cm} = 0$ and 180° with a discernible preference in the forward direction. The intensity of the sideways components is considerably smaller than that of the forward and backward ones. A qualitatively good agreement in the DCS is seen between the present and previous[23] QCT calculations at $E_{col} = 12.2$ kcal/mol, despite the fact that independent ab initio data set of the $1^1A'$ PES was employed. No marked E_{col} dependence is found in Figure 7a, except for the slight and nonmonotonic difference with respect to E_{col}. The variation of the calculated DCS within $E_{col} = 3.0-6.0$ kcal/mol is as small as the present experimental accuracy. Although the ground-state PES has been corroborated to have a deep double-well structure by ab initio calculations,[12,15,20−22] the fast dynamics without being trapped in the potential wells have been revealed,[19,23] resulting in the larger intensity in the forward direction. It is expected that the reaction mechanism is not significantly affected by the small difference of $E_{col} = 3-6$

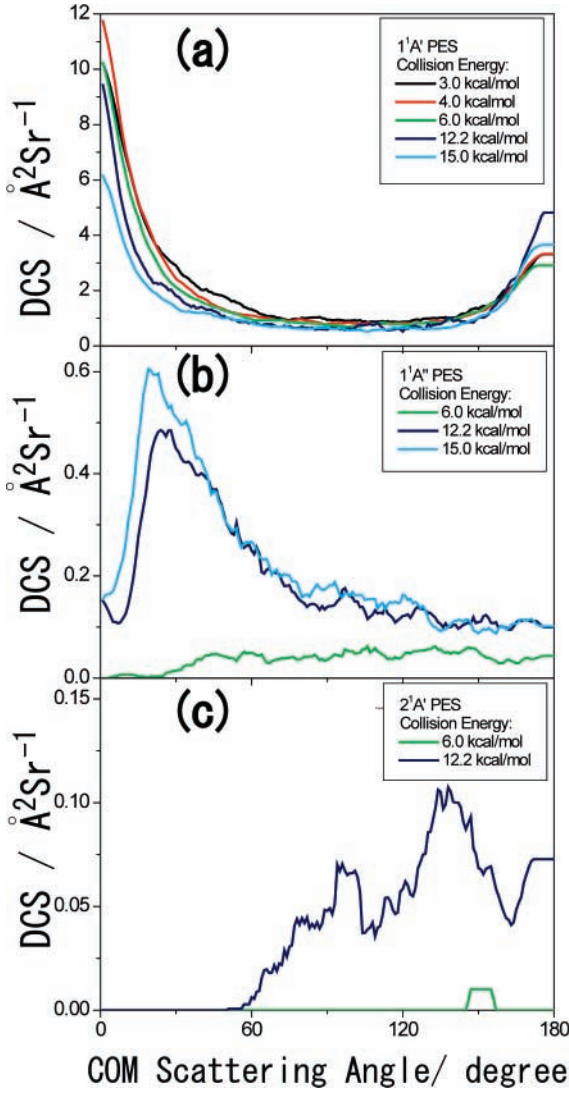

Figure 7. The theoretical differential cross sections of the O(^{1}D) + HCl → OH + Cl reaction obtained by the QCT calculation executed independently on (a) the $1^1A'$ ground-state PES, (b) the $1^1A''$ excited-state PES, and (c) the $2^1A'$ excited-state PES. The collision energy for each curve is designated with different colors in the legend, black for 3.0 kcal/mol, red for 4.0 kcal/mol, green for 6.0 kcal/mol, purple for 12.2 kcal/mol, and light blue for 15.0 kcal/mol.

kcal/mol because of the large exothermicity ($\Delta H_0 = -44.4$ kcal/mol) and the deep well structures (HOCl well depth: 101 kcal/mol) of the $1^1A'$ PES with no barrier. It is noted that the small E_{col} dependence of the theoretical DCS, especially the ratio between the forward and backward peaks, differs from the monotonic change expected from the osculating complex model. However, the present QCT results illustrate that the ground-state PES solely causes only a small variation of the DCS within a few kcal/mol width of E_{col}.

For discrimination between the reactions on the ground- and excited-state PESs, it is valuable to inspect an individual feature of the DCS on each PES prior to consideration of the coupling between PESs. The theoretical DCS on the $1^1A''$ PES (Figure 7b) shows a drastic change between $E_{col} = 6.0$ and 12.2 kcal/mol, the small intensity without the forward components at $E_{col} = 6.0$ kcal/mol and the increased intensity with a peak around $\theta_{cm} = 20°$ at $E_{col} = 12.2$ kcal/mol. The characteristic peak of the DCS is not simply explained by the height of the saddle point (1.6 kcal/mol) on the $1^1A''$ PES since it is bent. It seems that this bent saddle point does not play any significant

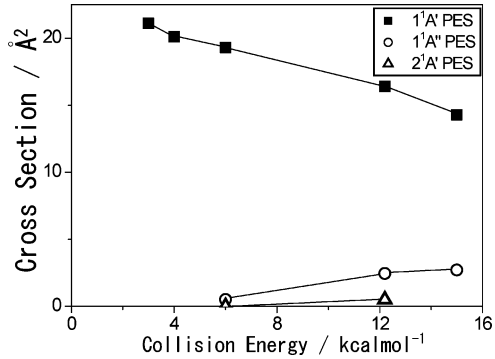

Figure 8. The theoretical reaction cross sections of the $O(^1D) + HCl \rightarrow OH + Cl$ reaction at the collision energies (E_{col}) of 3.0, 4.0, 6.0, 12.2, and 15.0 kcal/mol. These are the results obtained by QCT calculation executed independently on the $1^1A'$(■), $1^1A''$(○), and $2^1A'$(△) PESs. The data for the excited states at $E_{col} = 3.0$ and 4.0 kcal/mol are omitted because of their negligibly small magnitudes. The solid lines are guides for eyes.

role as a typical transition state in the dynamics. Another saddle point at $E_{col} = 16.1$ kcal/mol on the $1^1A''$ PES (Figure 6c) does not give any account either because it leads to the ClO + H pathway. At higher energies, the major reaction mechanism on the $1^1A''$ PES is speculated to occur over a wider interaction region than that of the potential barrier itself. On the other hand, the QCT results of the $2^1A'$ PES is consistent with a naïve expectation on the topographical basis of the PES; the saddle point associated with the collinear geometry at $E_{col} = 6.5$ kcal/mol yields the DCS which is characterized by backward scattering, as shown in Figure 7c. The collinear saddle point shown in Figure 6b is recognized to serve as an ordinary type of transition state. We found that the sum of the DCSs of the ground and the two excited states is almost the same as that of the ground state, indicating that contributions from the excited $1^1A''$ and $2^1A'$ states are negligible at the experimentally investigated energies.

The reaction cross sections (σ_{reac}) on each PES are shown in Figure 8. The σ_{reac} in the units of Å^2 is obtained by summing over each theoretical DCS with a multiplying factor of $2\pi\sin\theta_{cm}$. The σ_{reac}'s of the $1^1A'$, $1^1A''$, and $2^1A'$ states are independently calculated at particular E_{col}'s, which correspond to the partial excitation functions for the specific PESs, $\sigma_{reac}(E_{col}; \text{state})$. The $\sigma_{reac}(E_{col}; 1^1A'')$ and $\sigma_{reac}(E_{col}; 2^1A')$ at $E_{col} = 3.0$ and 4.0 kcal/mol are omitted since they are negligibly small. These theoretical $\sigma_{reac}(E_{col}; \text{state})$ provide a quantitative basis for the small contribution of the $1^1A''$ and $2^1A'$ excited states. The $\sigma_{reac}(E_{col}; 1^1A')$ behaves in a decreasing manner, which is typical for an attractive PES without a barrier. The relatively large magnitude (>10 Å^2) is naturally due to the widely extended interaction region over the double wells of the $1^1A'$ PES. The values of $\sigma_{reac}(E_{col}; 1^1A')$ in the same E_{col} region are consistent with the previous dynamics calculations by other authors, although the individual ab initio PES data for the $1^1A'$ PES were employed.[26,28−30,35] The QCT results predict that the contribution of the excited states emerges in the $E_{col} > 12$ kcal/mol region and becomes important probably at $E_{col} > 20$ kcal/mol. The ratio of σ_{reac} of the two excited states to that of the ground state, $[\sigma_{reac}(1^1A'') + \sigma_{reac}(2^1A')]/\sigma_{reac}(1^1A')$ is 0.03 at $E_{col} = 6.0$ kcal/mol and 0.23 at $E_{col} = 12.2$ kcal/mol. Although we also carried out the QCT calculations including tunneling effects[46] for all of the states and energies, the contribution due to tunneling effects was found to be negligibly small. A simple explanation based on the ab initio results is given to the relatively small $\sigma_{reac}(1^1A'')$ and $\sigma_{reac}(2^1A')$. A classical estimate of σ_{reac} is given by the integral of $2\pi bP(b)$ up to b_{peak}, where b_{peak} corresponds to the effective reaction barrier. Assuming that the b_{peak} is given by the saddle point, $b_{peak} \sim 1.0$ Å for the $1^1A''$ PES and $b_{peak} \sim 0$ Å for the $2^1A'$ PES are obtained from the ab initio calculations. The former value is obtained from the bent structure in the reactant region [R(H−Cl) = 1.31 Å compared with 1.27 Å of an isolated HCl],[47] and the latter are from the collinear saddle point. The small values of b_{peak} of the excited-state PESs are markedly contrasted with the $b_{peak} = 2.5$ Å of the $1^1A'$ PES, resulting in the considerably smaller $\sigma_{reac}(1^1A'')$ and $\sigma_{reac}(2^1A')$ than $\sigma_{reac}(1^1A')$.

Conclusion

The collision energy dependence of the $O(^1D) + HCl \rightarrow OH + Cl(^2P)$ reaction has been investigated both experimentally and theoretically. The doubly DCSs measured by the crossed molecular beam experiment in the $E_{col} = 4.2-6.4$ kcal/mol region exhibited nearly forward−backward symmetric distribution, with a pronounced forward component. The forward scattering was enhanced at the higher collision energies. The previous CASSCF-MRCI ab initio calculations predicted the existence of the reaction barrier of the $1^1A''$ (1.6 kcal/mol) and $2^1A'$ (6.5 kcal/mol) excited-state PESs. The QCT calculations were carried out separately on the ground-state ($1^1A'$) and the two excited-state ($1^1A''$, $2^1A'$) ab initio PESs. The calculated partial reaction cross section of the $1^1A'$ ground-state PES is much larger than those of the $1^1A''$ and $2^1A'$ states. This is because the excited-state pathways have reaction barriers and small cones of acceptance, while interactions in the ground-state pathway are attractive and provide a much larger cone of acceptance. The theoretical DCS of the ground-state $1^1A'$ PES is in good agreement with the experimental DCS. The present experimental and theoretical results conclude the dominant role of the reaction pathway via the ground-state $1^1A'$ PES at the collision energy below 6.5 kcal/mol.

Acknowledgment. This work was financially supported by Grant-in-Aid for Specially Promoted Research of the Ministry of Education, Culture, Sports, Science and Technology of Japan (No. 15002011). A part of the numerical calculations for the apparatus functions was carried out with use of the computer facilities at the RIKEN Super Combined Cluster (RSCC).

References and Notes

(1) Cheng, B. M.; Bahou, M.; Chen, W. C.; Yui, C. H.; Lee, Y. P.; Lee, L. C. *J. Chem. Phys.* **2002**, *117*, 1633.
(2) Dobbyn, A. J.; Knowles, P. J. *Mol. Phys.* **1997**, *91*, 1107.
(3) Kassab, E.; Gleghorn, J. T.; Evleth, E. M. *J. Am. Chem. Soc.* **1983**, *105*, 1746.
(4) Lin, J. J.; Harich, S.; Lee, Y. T.; Yang, X. *J. Chem. Phys.* **1999**, *110*, 10821.
(5) Suzuki, T.; Hirota, E. *J. Chem. Phys.* **1993**, *98*, 2387.
(6) Hermine, P.; Hsu, Y. T.; Liu, K. *Phys. Chem. Chem. Phys.* **2000**, *2*, 581.
(7) Hsu, Y. T.; Liu, K.; Pederson, L. A.; Schatz, G. C. *J. Chem. Phys.* **1999**, *111*, 7931.
(8) Hsu, Y. T.; Wang, J. H.; Liu, K. *J. Chem. Phys.* **1997**, *107*, 2351.
(9) Schatz, G. C.; Papaioannou, A.; Pederson, L. A.; Harding, L. B.; Hollebeek, T.; Ho, T. S.; Rabitz, H. *J. Chem. Phys.* **1997**, *107*, 2340.
(10) Hsu, Y. T.; Liu, K.; Pederson, L. A.; Schatz, G. C. *J. Chem. Phys.* **1999**, *111*, 7921.
(11) Hirsch, G.; Bruna, P. J.; Peyerimhoff, S. D.; Buenker, R. J. *Chem. Phys. Lett.* **1977**, *52*, 442.
(12) Bruna, P. J.; Hirsch, G.; Peyerimhoff, S. D.; Buenker, R. J. *Can. J. Chem.* **1979**, *57*, 1839.
(13) Nanbu, S.; Iwata, S. *J. Phys. Chem.* **1992**, *96*, 2103.
(14) Guo, H. *J. Phys. Chem.* **1993**, *97*, 2602.
(15) Nanbu, S.; Aoyagi, M.; Kamisaka, H.; Nakamura, H.; Bian, W.; Tanaka, K. *J. Theor. Comput. Chem.* **2002**, *1*, 263.
(16) Park, C. R.; Wiesenfeld, J. R. *Chem. Phys. Lett.* **1989**, *163*, 230.

(17) Matsumi, Y.; Tonokura, K.; Kawasaki, M.; Tsuji, K.; Obi, K. *J. Chem. Phys.* **1993**, *98*, 8330.
(18) Kruus, E. J.; Niefer, B. I.; Sloan, J. J. *J. Chem. Phys.* **1988**, *88*, 985.
(19) Kohguchi, H.; Suzuki, T. *ChemPhysChem* **2006**, *7*, 1250.
(20) Peterson, K. A.; Skokov, S.; Bowman, J. M. *J. Chem. Phys.* **1999**, *111*, 7446.
(21) Hernandez, M. L.; Redondo, C.; Lagana, A.; deAspuru, G. O.; Rosi, M.; Sgamellotti, A. *J. Chem. Phys.* **1996**, *105*, 2710.
(22) Lee, T. J. *J. Phys. Chem.* **1994**, *98*, 3697.
(23) Martínez, T.; Hernandez, M. L.; Alvarino, J. M.; Aoiz, F. J.; Rabanos, V. S. *J. Chem. Phys.* **2003**, *119*, 7871.
(24) Kamisaka, H.; Nakamura, H.; Nanbu, S.; Aoyagi, M.; Bian, W.; Tanaka, K. *J. Theor. Comput. Chem.* **2002**, *1*, 285.
(25) Kamisaka, H.; Nakamura, H.; Nanbu, S.; Aoyagi, M.; Bian, W.; Tanaka, K. *J. Theor. Comput. Chem.* **2002**, *1*, 275.
(26) Christoffel, K. M.; Bowman, J. M. *J. Chem. Phys.* **2002**, *116*, 4842.
(27) Piermarini, V.; Lagana, A.; Balint-Kurti, G. G. *Phys. Chem. Chem. Phys.* **2001**, *3*, 4515.
(28) Piermarini, V.; Balint-Kurti, G. G.; Gray, S. K.; Gogtas, F.; Lagana, A.; Hernandez, M. L. *J. Phys. Chem. A* **2001**, *105*, 5743.
(29) Martínez, T.; Hernandez, M. L.; Alvarino, J. M.; Lagana, A.; Aoiz, F. J.; Menendez, M.; Verdasco, E. *Phys. Chem. Chem. Phys.* **2000**, *2*, 589.
(30) Lin, S. Y.; Han, K. L.; Zhang, J. Z. H. *Phys. Chem. Chem. Phys.* **2000**, *2*, 2529.
(31) Lin, S. Y.; Han, K. L.; Zhang, J. Z. H. *Chem. Phys. Lett.* **2000**, *324*, 122.
(32) Bittererova, M.; Bowman, J. M. *J. Chem. Phys.* **2000**, *113*, 1.
(33) Alvarino, J. M.; Rodriguez, A.; Lagana, A.; Hernandez, M. L. *Chem. Phys. Lett.* **1999**, *313*, 299.
(34) Lagana, A.; Deaspuru, G. O.; Garcia, E. *J. Phys. Chem.* **1995**, *99*, 17139.
(35) Schinke, R. *J. Chem. Phys.* **1984**, *80*, 5510.
(36) Kohguchi, H.; Suzuki, T.; Alexander, M. H. *Science* **2001**, *294*, 832.
(37) *MOLPRO* is a package of ab initio programs written by Werner, H.-J.; Knowles, P. J.; Schüetz, M.; Lindh, R.; Celani, P.; Korona, T.; Rauhut, G.; Manby, F. R.; Amos, R. D.; Bernhardsson, A.; Berning, A.; Cooper, D. L.; Deegan, M. J. O.; Dobbyn, A. J.; Eckert, F.; Hampel, C.; Hetzer, G.; Lloyd, A. W.; McNicholas, S. J.; Meyer, W.; Mura, M. E.; Nicklass, A.; Palmieri, P.; Pitzer, R.; Schumann, U.; Stoll, H.; Stone, A. J.; Tarroni, R.; Thorsteinsson, T. Version: 2006.1, URL: http://www.molpro.net.
(38) Ishida, T.; Schatz, G. C. *Chem. Phys. Lett.* **1999**, *314*, 369.
(39) Chichinin, A. I. *J. Chem. Phys.* **1997**, *106*, 1057.
(40) Luntz, A. C. *J. Chem. Phys.* **1980**, *73*, 5393.
(41) Basco, N.; Norrish, R. G. W. *Proc. R. Soc. London. Ser. A* **1960**, *260*, 293.
(42) Christoffel, K. M.; Kim, K.; Skokov, S.; Bowman, J. M.; Gray, S. K. *Chem. Phys. Lett.* **1999**, *315*, 275.
(43) Alagia, M.; Balucani, N.; Casavecchia, P.; Stranges, D.; Volpi, G. G. *J. Chem. Phys.* **1993**, *98*, 8341.
(44) Fisk, G. A.; McDonald, J. D.; Herschbach, D. R. *Discuss. Faraday Soc.* **1967**, *44*, 228.
(45) Che, D.; Liu, K. *J. Chem. Phys.* **1995**, *103*, 5164.
(46) Oloyede, P.; Mil'nikov, G.; Nakamura, H. *J. Theor. Comput. Chem.* **2004**, *3*, 91.
(47) Herzberg, G. *Molecular Spectra and Molecular Structure I. Spectra of Diatomic Molecules*, 2nd ed.; Krieger: Malabar, Florida, 1950.